Semiconducting Electronic Property of Graphene Adsorbed on (0001) Surfaces of SiO_2

Nguyen Thanh Cuong,[1,3] Minoru Otani,[1,3] and Susumu Okada[2,3]

[1]*Nanosystem Research Institute (NRI), National Institute of Advanced Industrial Science and Technology (AIST), Tsukuba 305-8568, Japan*

[2]*Graduate school of Pure and Applied Sciences, University of Tsukuba, 1-1-1 Tennodai, Tsukuba 305-8571, Japan*

[3]*Japan Science and Technology Agency, CREST, 5 Sanbancho, Chiyoda-ku, Tokyo 102-0075, Japan*

(Received 8 September 2010; revised manuscript received 7 January 2011; published 7 March 2011)

First-principles total energy calculations are performed to investigate the energetics and electronic structures of graphene adsorbed on both an oxygen-terminated SiO_2 (0001) surface and a fully hydroxylated SiO_2 (0001) surface. We find that there are several stable adsorption sites for graphene on both O-terminated and hydroxylated SiO_2 surfaces. The binding energy in the most stable geometry is found to be 15 meV per C atom, indicating a weak interaction between graphene and SiO_2 (0001) surfaces. We also find that the graphene adsorbed on SiO_2 is a semiconductor irrespective of the adsorption arrangement due to the variation of on-site energy induced by the SiO_2 substrate.

DOI: 10.1103/PhysRevLett.106.106801 PACS numbers: 73.22.Pr, 61.48.Gh, 71.15.Mb, 81.05.ue

Exfoliation of graphite [1,2] and thermal annealing of SiC [3,4] have now achieved the single-layered graphite, graphene, which provides us a perfect two-dimensional electronic system. Much effort has been devoted not only to the elucidation of fundamental physics on this new and famous carbon allotrope but also to the exploration of the possibility of application in the next generation of electronic devices [1,5–9]. Graphene possesses a pair of linear dispersion bands at the Fermi level resulting in remarkable carrier mobility of a few hundred thousand $cm^2/V\,s$, and leading to application of graphene in high-speed switching devices [1,5–10]. On the other hand, these remarkable electronic properties of graphene have been shown to be vulnerable to external conditions such as structural corrugations, atom or molecule adsorptions, and interactions with other graphene or substrate surfaces [8–13]. Although this issue may be fatal to the application of graphene as a switching device in semiconductors, graphene is still applicable as a constituent of sensing devices. From both the fundamental precise two-dimensional physics and applied semiconductor engineering points of view, it is important to elucidate the effects of other materials on the electronic and structural properties of graphene.

Hybrid structures of graphene with insulating substrates are important for both fundamental studies and applications of graphene. Silicon dioxide (SiO_2) is widely used as an insulating substrate for device fabrication and physical property measurement. Many experiments reported the modulation of the electronic properties of graphene on a SiO_2 substrate, such as band gap opening and decrease of carrier mobility [8–10]. The interaction between the graphene and substrate is considered to play a crucial role in the modulation. Although many theoretical calculations [14–16] have been performed to elucidate the fundamental properties of graphene adsorbed on SiO_2 surfaces, there is still no clear physical insight into the fundamental properties of this hybrid system. Therefore, in the present work, we aim to investigate theoretically the energetics and electronic structures of graphene adsorbed on (0001) surfaces of α quartz using realistic and physical surface atomic structures based on first-principles total energy calculations in the framework of density functional theory. Our calculations clearly show that graphene keeps its plane structure, and is weakly bound to the substrate without forming covalent bond with O/Si atoms. The calculated binding energy calculated is about 10 meV per C atom. We also found that the graphene has semiconducting properties with a direct band gap of a few tens of meV. Detailed analysis of the local electrostatic potential reveals that the semiconducting properties are ascribed to the modulation of on-site energy of C atoms induced by the substrate.

All calculations have been performed based on density functional theory [17,18]. We use the local density approximation (LDA) to express the exchange-correlation energy of interacting electrons [19,20]. Ultrasoft pseudopotentials are adopted to describe the electron-ion interaction [21]. The valence wave functions and charge density are expanded in terms of a plane-wave basis set with cutoff energies of 25 and 225 Ry, respectively. The Brillouin-zone integration is performed with a $6 \times 6 \times 1$ k mesh for geometry optimization and with a $12 \times 12 \times 1$ k mesh for self-consistent electronic structure calculations for band dispersion. Geometry optimization has been performed for all atoms in the slab, until the remaining force acting on atoms is less than 0.005 Ry/Å. The conjugated-gradient minimization scheme is used for both the electronic structure calculation and for the geometry optimization.

The surfaces are simulated using a repeated-slab model in which 9 Si atomic layers of α quartz, graphene, and a 10 Å-vacuum region are included. We chose (0001)

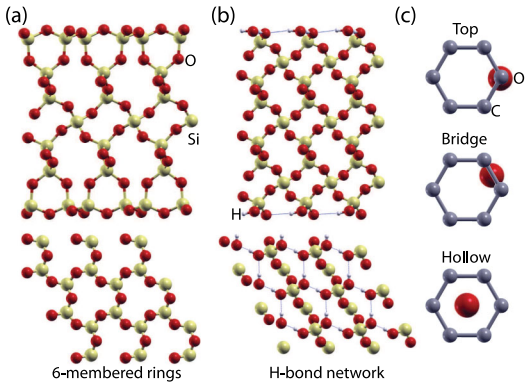

FIG. 1 (color online). Side and top views of reconstructed structures of (a) O-terminated SiO_2 (0001) surface, and (b) fully hydroxylated SiO_2 (0001) surface. The hydrogen bonds are shown in dashed lines. (c) Three representative arrangements of graphene on SiO_2: top (T) configuration, bridge (B) configuration, and hollow (H) configuration.

surfaces of α quartz as a model surface of SiO_2 on which to adsorb the graphene. To avoid periodic image errors arising from the slab model, we adopt the effective-screening medium method [22,23]. We do not consider simple cleaved surfaces (as used for previous calculations) [14–16] but fully optimized oxygen-terminated (0001) surfaces to simulate experimentally relevant situations. Previous experimental and theoretical studies [24,25] have shown that the upper or lower two subsurfaces of cleaved SiO_2 undergo surface reconstruction at around 300 K to give O-terminated surfaces with six-membered rings as shown in Fig. 1(a). Besides these O-terminated surfaces, cleaved surfaces will also be rapidly hydroxylated under ambient conditions, yielding silanol groups (Si-OH) [25–27]. Thus, in this Letter, we also consider the fully hydroxylated SiO_2 surface possessing a zigzag hydrogen bonded network [Fig. 1(b)]. On these surfaces, we put graphene with 2×2 lateral periodicity to keep the commensurability condition with the lateral cell of SiO_2 (less than 0.08% lattice mismatch). To investigate how the energetics and electronic structure of graphene depend on the local configuration on SiO_2, we considered three representative arrangements of graphene on SiO_2 where an oxygen atom (from either the reconstructed O-terminated or hydroxylated surface) is situated directly below either: a C atom, the center of a C-C bond, or the hollow site at the center of the C hexagonal ring, which are classified as the top (T), the bridge (B), and the hollow (H) configurations, respectively, as shown in Fig. 1(c).

Figures 2(a)–2(c) show the fully optimized geometric structures of graphene adsorbed on O-terminated SiO_2 surfaces. In all cases, graphene keeps its plane and hexagonal atomic network, maintaining the spacing of 2.9 Å for T, B, and H configurations, when bound to the SiO_2 surfaces. Of the three configurations, the hollow one is the most stable. The calculated binding energy per C atom of

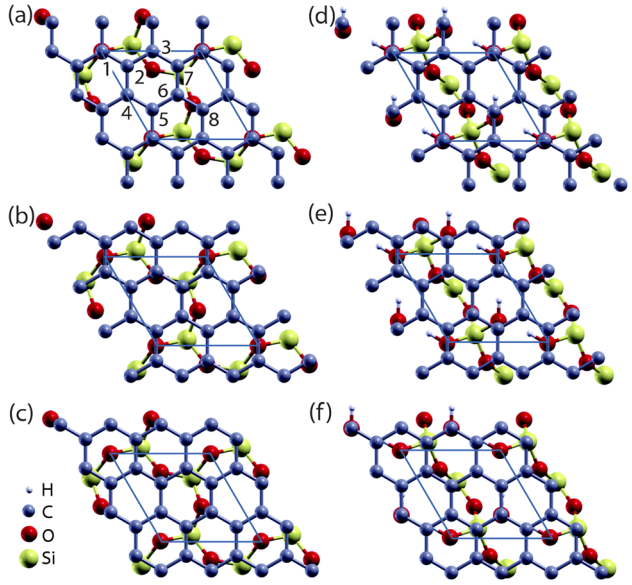

FIG. 2 (color online). Top views of optimized structures of graphene on (a) top, (b) bridge, (c) hollow sites of O-terminated SiO_2 (0001) surface, and on (d) top, (e) bridge, (f) hollow sites of fully hydroxylated SiO_2 (0001) surface. The surface unit cell is shown by the solid lines. The indexes of C atoms in the unit cell are used in the Tables III and IV.

H configuration is 15 meV, about 3 meV greater than that of the other two configurations (Table I). These results indicate that the energetics of graphene on O-terminated surfaces are not very sensitive to the adsorption site [28].

We also find similar optimized structures and energetics for graphene on fully hydroxylated SiO_2 surface. As shown in Figs. 2(d)–2(f), graphene essentially retains its initial structure with separations of about 2.93 Å for all configurations. The binding energies of graphene on hydroxylated surfaces are 8, 10.7, and 13 meV for T, B, and H configurations, respectively. Thus, as for the O-terminated surface, graphene is loosely bound to the surface without any site selectivity.

These energetics of adsorption of graphene on both O-terminated and hydroxylated surfaces correspond well

TABLE I. Equilibrium distance d_0(Å) and binding energy E_b (meV/C atom) of graphene on different adsorption sites of O-terminated and hydroxylated SiO_2 (0001) surfaces. Equilibrium distance d_0 is the distance between graphene layer and topmost atom in SiO_2 slab. The E_b is estimated by the equation $E_b = E_G + E_{SiO} - E_{G/SiO}$, where E_G, E_{SiO}, and $E_{G/SiO}$ are total energies of the isolated graphene, isolated SiO_2 slab, and graphene-SiO_2 hybrid systems, respectively.

	O terminated		Hydroxylated	
Adsorption site	d_0	E_b	d_0	E_b
Top	2.88	11.1	2.96	8.3
Bridge	2.90	10.9	2.93	10.7
Hollow	2.89	14.6	2.91	12.8

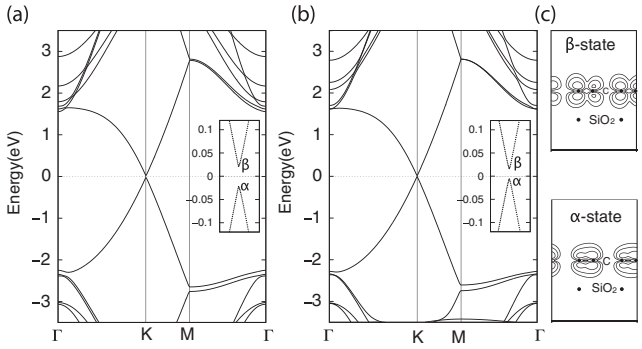

FIG. 3. Electronic energy band of graphene on (a) O-terminated SiO_2 (0001) surface, and on (b) hydroxylated SiO_2 (0001) surface. The insets are expansions of the bands around the K point. (c) Contour plots of the square wave function of the states denoted by α and β in the insets.

with the previous experimental work [29], in which the binding energy was determined to be 16 meV per C atom. However, the spacing between the graphene and the surfaces was about 1.3 Å larger than those spacings obtained in our calculations. This structural discrepancy probably arises from the difference between the model SiO_2 structure used in the calculation and the amorphous SiO_2 used in the experiment. For instance, the nanometer scale structures on SiO_2, such as steps and adsorbates of environmental materials, lead the larger spacing between graphene and substrates. It must be pointed out that our results are inconsistent with previous theoretical results, in which a graphene monolayer is found to bound strongly to O-terminated SiO_2 surfaces via covalent bonds [14–16]. In the previous calculations, graphene has been adsorbed on cleaved SiO_2 surfaces which have unsaturated O dangling bonds that can easily form a covalent CO bond, and hence lead to the different energetics and adsorbed structures. It has been experimentally established that graphene is weakly bound to SiO_2 substrates via van der Waals and/or capillary forces [1]. Therefore, our results on energetics and atomic structures agree with the experimental results. From our calculations, we also estimate the energy cost for the corrugation of graphene as a few meV per C atom. Thus, the interaction between graphene and SiO_2 surfaces is sufficient to overcome the energy cost for the corrugation of graphene. In other words, the structure of graphene follows the morphology of the SiO_2 substrates.

TABLE II. Band gap (meV) of monolayer graphene and bilayer graphene on different adsorption sites of O-terminated and hydroxylated (0001) surfaces of SiO_2.

	O terminated		Hydroxylated	
Adsorption site	Monolayer	Bilayer	Monolayer	Bilayer
Top	44	4	11	1
Bridge	29	1	13	0
Hollow	18	6	23	0

TABLE III. Electrostatic potential of each C atom of graphene on O-terminated (0001) surface of SiO_2. The energy (meV) is measured from the electrostatic potential of C atom in isolated graphene. Indexes correspond with the C atomic sites denoted in Fig. 2(a).

	C_1	C_2	C_3	C_4	C_5	C_6	C_7	C_8
Top	69	67	71	78	69	81	63	58
Bridge	44	74	51	51	77	51	73	73
Hollow	56	61	70	51	74	69	63	63

Next, we focus on the electronic structures of graphene on the SiO_2 surfaces. Figures 3(a) and 3(b) show the electronic energy band of the graphene adsorbed on the O-terminated and hydroxylated (0001) surfaces of SiO_2. On both SiO_2 surfaces, the character of the electronic energy band of pristine monolayer graphene seems to be preserved. However, focusing on the Dirac cone at the K point, reveals that the π and π^* bands repulse each other, forming a small energy gap at the K point as shown in the insets of Figs. 3(a) and 3(b). Thus, the graphene adsorbed on the SiO_2 surfaces is no longer metallic with massless electrons, but semiconducting with a direct narrow fundamental gap. Table II lists the calculated gaps of graphene with different adsorption sites on O-terminated and hydroxylated SiO_2 surfaces. We find that the band gaps of graphene on the O-terminated SiO_2 (0001) surface are larger than those on the fully hydroxylated SiO_2 surfaces. The band gaps are found to be 11–44 meV depending on the adsorption arrangement of graphene and the surface structures of SiO_2, despite the energetics and geometric structure of graphene on SiO_2 being largely independent of adsorption arrangement. These gap values are comparable to the band gaps obtained for graphene on hexagonal boron nitride or Cu(111) surface [30,31]. Furthermore, the values are significantly higher than k_BT at room temperature so that the adsorption decreases the transport properties of graphene compared with the free standing graphene.

The semiconducting properties of graphene on SiO_2 imply that the on-site energy of C atoms is modulated by the adsorption and depends on the mutual arrangement relavtive to the O atoms on the surfaces. To further investigate this, we analyzed the electrostatic potential of C atoms of graphene on SiO_2 surfaces. We found that there

TABLE IV. Electrostatic potential of each C atom of graphene on hydroxylated (0001) surface of SiO_2. The energy (meV) is measured from the electrostatic potential of C atom in isolated graphene. Indexes correspond with the C atomic sites denoted in Fig. 2(a).

	C_1	C_2	C_3	C_4	C_5	C_6	C_7	C_8
Top	120	126	119	142	134	144	127	117
Bridge	103	124	108	96	110	95	128	109
Hollow	104	137	104	126	163	142	136	161

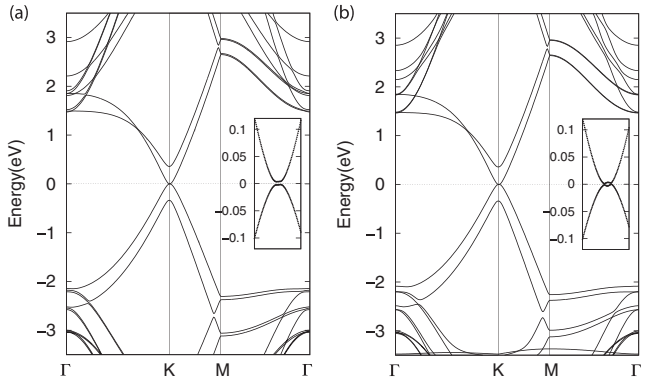

FIG. 4. Electronic energy band of bilayer graphene on (a) O-terminated SiO_2 (0001) surface, and on (b) hydroxylated SiO_2 (0001) surface. The insets are expansions of bands around the K point.

is spatial inhomogeneity in the electrostatic potential of C atoms of graphene. Indeed, the electrostatic potential on graphene adsorbed on SiO_2 strongly depends on the C sites and is shallower by 59–100 meV than that of C atoms belonging in isolated graphene [Tables III and IV]. The variation of the electrostatic potential is 23 and 45 meV for graphene on O-terminated and hydroxylated SiO_2 (0001) surfaces with on-top arrangements, respectively. These values are the same order as the gap energy of graphene on SiO_2. Indeed, single orbital tight-binding calculations for isolated graphene with on-site energy variation result in the energy gap of 10 meV at K point. Thus, we conclude that the variation in electrostatic potential or on-site energy of C atoms disrupts the degeneracy of the π and π^* bands at the K point resulting in their semiconducting character. The on-site energy difference can be observed in the wave functions from the top of valence band [α state in Fig. 3(c)] and the bottom of the conduction band [β state in Fig. 3(c)] at the K point. The distribution of the wave function of the π state in graphene is not equivalent between adjacent C atoms as in the case of hexagonal boron nitride which exhibit π bonding character. The inhomogeneous on-site energy of the C atoms is induced not by the charge transfer between the graphene and the surfaces but by the inhomogeneous charge distribution on the SiO_2 surfaces. Indeed, our analyses of charge distribution show that there is no charge transfer to or from graphene. The charge redistribution occurs only at the interfacial region, and induces very small dipole moments.

Next, we investigate the electronic properties of bilayer graphene on SiO_2 surfaces. We find that the equilibrium interlayer distance with AB stacking arrangement is 3.35 Å. Figures 4(a) and 4(b) show the electronic energy band of bilayer graphene adsorbed on O-terminated and hydroxylated SiO_2 surfaces. These systems exhibit the parabolic bands around the Fermi level which resemble those of pristine bilayer graphene. Detailed analyses of the electronic energy bands around the Fermi level revealed that a small band gap of less than 6 meV is still opened [see the inset of Fig. 4(a)]. The band gap values of bilayer graphene with different configurations on both O-terminated and hydroxylated SiO_2 surfaces are listed in Table II. However, these band gaps are within the accuracy limitation of the LDA, and therefore we can assume that the band gap value is zero. Thus, the zero gap of the graphene layer is recovered when a second graphene layer is placed.

This work was partly supported by CREST, Japan Science and Technology Agency, and a Grant-in-Aid for scientific research from the Ministry of Education, Culture, Sports, Science and Technology of Japan.

[1] K. S. Novoselov *et al.*, Science **306**, 666 (2004).
[2] A. K. Geim and K. S. Novoselov, Nature Mater. **6**, 183 (2007).
[3] I. Forbeaux, J.-M. Themlin, and J.-M. Debever, Phys. Rev. B **58**, 16 396 (1998).
[4] C. Berger *et al.*, Science **312**, 1191 (2006).
[5] K. S. Novoselov *et al.*, Nature (London) **438**, 197 (2005).
[6] Y. Zhang *et al.*, Nature (London) **438**, 201 (2005).
[7] M. Otani *et al.*, Phys. Rev. B **81**, 161403(R) (2010).
[8] J. B. Oostinga *et al.*, Nature Mater. **7**, 151 (2007).
[9] Y. Zhang *et al.*, Nature (London) **459**, 820 (2009).
[10] M. F. Craciun *et al.*, Nature Nanotech. **4**, 383 (2009).
[11] T. Ohta *et al.*, Science **313**, 951 (2006).
[12] S. Y. Zhou *et al.*, Nature Mater. **6**, 770 (2007).
[13] A. Mattausch and O. Pankratov, Phys. Rev. Lett. **99**, 076802 (2007).
[14] Y.-J. Kang, J. Kang, and K. J. Chang, Phys. Rev. B **78**, 115404 (2008).
[15] M. Z. Hossain, Appl. Phys. Lett. **95**, 143125 (2009).
[16] P. Shemella and S. K. Nayak, Appl. Phys. Lett. **94**, 032101 (2009).
[17] P. Hohenberg and W. Kohn, Phys. Rev. **136**, B864 (1964).
[18] W. Kohn and L. J. Sham, Phys. Rev. **140**, A1133 (1965).
[19] D. M. Ceperley and B. J. Alder, Phys. Rev. Lett. **45**, 566 (1980).
[20] J. P. Perdew and A. Zunger, Phys. Rev. B **23**, 5048 (1981).
[21] D. Vanderbilt, Phys. Rev. B **41**, 7892 (1990).
[22] M. Otani and O. Sugino, Phys. Rev. B **73**, 115407 (2006).
[23] I. Hamada *et al.*, Phys. Rev. B **80**, 165411 (2009).
[24] G.-M. Rignanese *et al.*, Phys. Rev. B **61**, 13 250 (2000).
[25] T. P. M. Goumans *et al.*, Phys. Chem. Chem. Phys. **9**, 2146 (2007).
[26] G.-M. Rignanese *et al.*, Phys. Chem. Chem. Phys. **6**, 1920 (2004).
[27] J. Yang and E. G. Wang, Phys. Rev. B **73**, 035406 (2006).
[28] It should be noted that LDA well reproduces the interunit spacing of van der Waals materials.
[29] M. Ishigami *et al.*, Nano Lett. **7**, 1643 (2007).
[30] G. Giovannetti *et al.*, Phys. Rev. B **76**, 073103 (2007).
[31] S. Okada, Jpn. J. Appl. Phys. **49**, 020204 (2010).